

# Simulation Study of a Novel Subgrid Model for Microtopography Effect on Surface Flow

---

## Abstract

In permafrost-affected regions, subsurface is mainly characterized by ice-wedge polygons that form a patterned polygonal ground. The role of patterned polygonal ground and the associated fine-scale microtopography (at a scale smaller than the size of polygons) in controlling surface/subsurface thermal hydrology is critical but well-understood. Fine-scale simulations are required to capture microtopographic influences on flow. Standalone fine-scale surface hydrology simulations are feasible with modern computing tools. However, highly resolved integrated surface/subsurface thermal hydrology simulations are not tractable at watershed scale and requires proper modeling. To capture the effects of microtopography (depressions, obstructions etc.) in coarsened model, we present a subgrid model parameterized by fine-scale microtopographic features, which alters the water storage and flow terms in the governing equations. Simulations were carried out and numerical results of the subgrid model were compared both to those generated with no subgrid model and to fine-scale results of seven ice-wedge polygons. Our findings confirm that the subgrid model improves the shape of the hydrographs and the total water content in the system, and that the results are very close to the corresponding fine-scale simulations. Watershed-scale fully integrated surface/subsurface simulations with the subgrid model show that the surface depressions increase infiltration and reduce runoff, thereby

highlighting the microtopographic effects on the watershed-scale hydrology. Finally, our work explores how parameters can be deduced from the available fine-scale information to account for microtopographic effects in coarsened integrated models.

*Keywords:* Subgrid model, Permafrost, Polygonal tundra, Microtopography, Watershed, Integrated Surface/Subsurface

---

## 1. Introduction

The Arctic landscapes are dominated by polygonal patterned (inter-connected polygons) ground. The formation of polygonal landscapes in permafrost-affected regions is a consequence of recurring cracks-compression  
5 process over hundreds of thousands of years. During winter, vertical fractures are formed due to ground contraction, the water from the snowmelt in the following summer penetrates those cracks and refreezes. In the following winter, the reexpansion of the ice in the cracks compresses the soil horizontally. The recurring crack-compression process over long period of time develops wedges of ice and finally a polygonal landscape is formed [1, 2, 3, 4].  
10 Figure 1 displays a polygonal tundra, which is a field site of the U.S. Department of Energy’s Next Generation Ecosystem Experiments (NGEE) Arctic project located within the Barrow Environmental Observatory (BEO) [5]. Several types of polygons are formed due to permafrost degradation. Typically, the polygons are classified as low-centered polygon (LCP) and high-centered polygon (HCP) based on surface microtopography. The LCP has a raised rim and central depression, thereby holds ponded water in the center during the summer that can only be available for infiltration and evaporation. The HCP has elevated center that slopes downward to trough and  
15

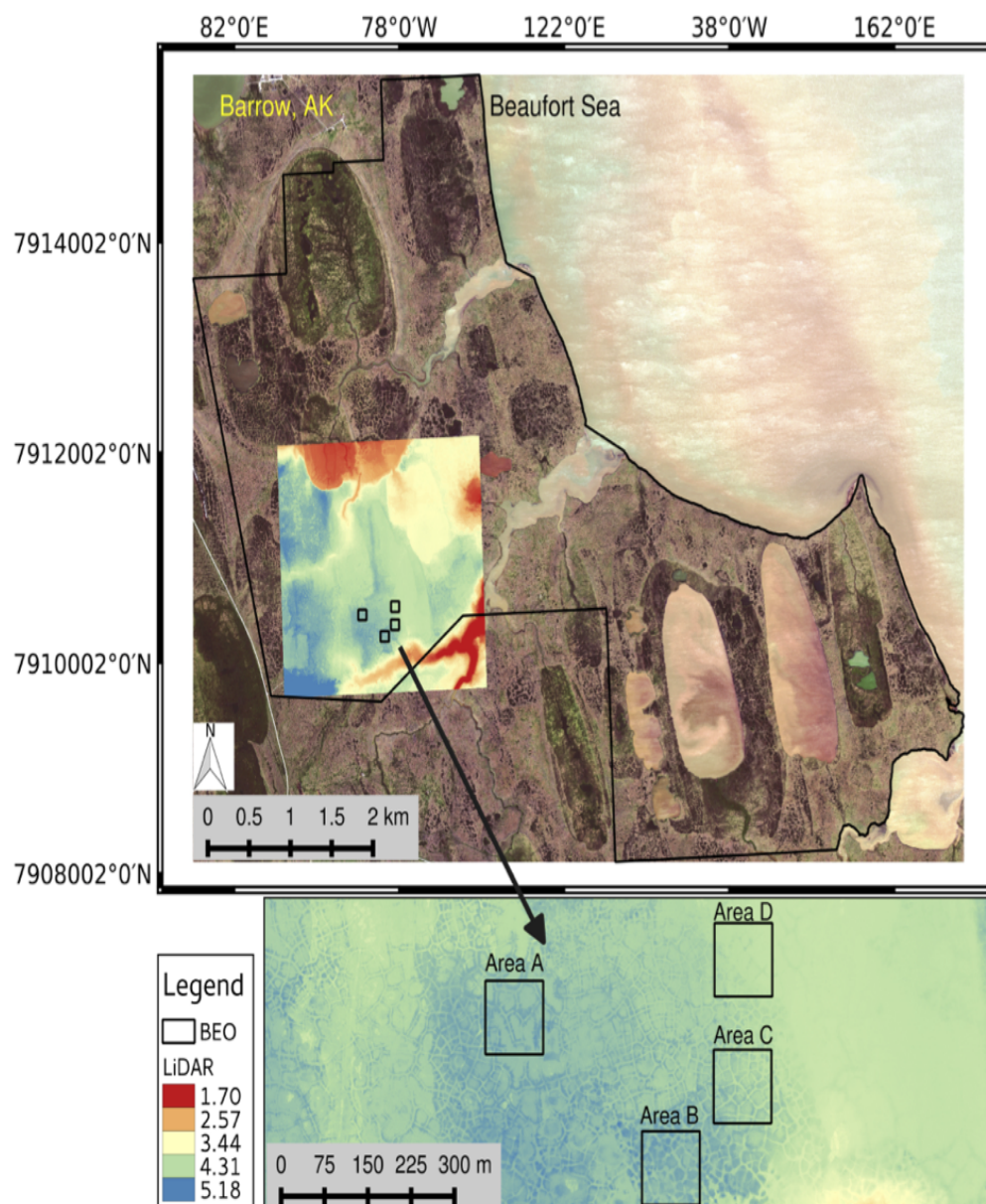


Figure 1: NGEE-Arctic field sites at BEO [5].

20 enhances runoff, thus the center may remain mostly dry. Thawing of ice-  
 wedges causes the raised rims of LCP to subside that leads to the formation  
 of HCP [6]. The loss of depression storage in the LCP has the ability to  
 connect the disconnected troughs, thus transforms a poorly drained tundra  
 to a well-established drainage network. Those changes will potentially alter  
 25 the entire ecosystem and will bring substantial hydrological changes (e.g.,  
 surface/subsurface interactions, distribution of surface water, discharge rate  
 etc.) [7, 8, 9]. To better understand the interactions between surface and  
 subsurface, surface runoff and discharge rate, it is important to gain in-  
 sight into the role of heterogeneous spatial structure of the ground surface.  
 30 It is well understood that the spatial heterogeneity in the surface micro-  
 topography (unevenness at small scale) serves a critical role in the sur-  
 face water retention, surface/subsurface interactions, and delay runoff, and  
 thereby significantly affects the shape of hydrographs [10][**References**]. In  
 general, an accurate flow representation is achieved at fine-scale (a scale  
 35 of centimeters) and fortunately with the availability of sophisticated simu-  
 lation tools, standalone highly resolved surface-flow simulations are easily  
 tractable. However, fully integrated surface/subsurface thermal hydrology  
 simulations with highly resolved computational grid are not tractable at  
 watershed scale. Hence the processes representing flow will not be accurate  
 40 if the microtopographic effects are ignored in the integrated models. The  
 idea to incorporate fine-scale flow behavior in the watershed-scale integrated  
 models motivates the use of subgrid representation. A subgrid model is build  
 on the information gained from highly resolved surface topographic data:  
 the depressions and obstructions. Depressions are disconnected low points  
 45 in the topography (surface pits) that retain water that is available only for  
 infiltration or/and evaporation. Obstructions are objects exit above the de-

50 pressions that interrupt and slow the flow, but do not completely block it. To incorporate the microtopographic features in the governing equations, the accumulation term is altered to account for depressions, and a modified flow law is used to introduce obstructions; more details are provided in the subsequent sections. are used in the flow law to introduce obstructions. This alteration of terms yield subgrid models. It is worth to point out, that we intend to use the subgrid parametrization with a mixed-dimensional model reported here [11], where the subsurface is discretized as independent
 55 columns and coupled through a surface flow system. In this work, the subgrid parameterization is applied to the lateral flow part only, which is the surface system. This is one aspect of incorporating the microtopographic effects in watershed-scale integrated models, however, in general, both the surface and subsurface require a subgrid model.

60 Pertinent to the literature, integrated surface/subsurface modeling has received considerable attention from researchers across the world; see, for example, [12, 13, 14] and references therein. Here we focus only on the subgrid modeling approach. Though the concept of microtopographic features and their implications on the flow and discharge is not new, but has not been fully
 65 addressed and understood from modeling perspective. Accurate representation of surface microtopography in a coupled surface/subsurface hydrologic model at watershed-scale is a challenging task. In the mid-1950s, the significance of the surface microtopographic features were described in [15]. A one-dimensional simulations to study the effects of spatially varying surface
 70 roughness on flow hydrographs is presented in [10]. Panday and Huyakorn (2004) presented an integrated surface/subsurface flow model with subgrid representation through the surface depressions and obstructions by modifying the overland flow governing equation. **INCOMPLETE!!**

The rest of the paper is organized as follows. Section 2 introduces the  
75 derivation of the governing equations of the subgrid model. A short descrip-  
tion, for a quick reference, of the Advanced Terrestrial Simulator (ATS)  
and the Arcos multiphysics management framework, within which we im-  
plemented our subgrid model, is presented in Section 3. In Section 4 we  
compare the numerical results of our subgrid model with no subgrid model  
80 and fine-scale results to illustrate the accuracy of our subgrid model for cap-  
turing fine-scale microtopographic features. Finally, in Section 5, we offer  
closing remarks and future research inline with thaw-induced subsidence.

## 2. Subgrid Model

This section describes the derivation of the subgrid model. The subgrid  
model alters the accumulation term and the flow law. For example, the  
ponded depth in the accumulation term is typically replaced with a volu-  
metric depth, the ponded depth that would occur if the surface were flat.  
Specifically, we make the substitution in the accumulation term, where is  
ponded depth. The volumetric head may be calculated on geometric argu-  
ments. Specifically, if the microtopographic elevation field on an ice-wedge  
polygon (IWP) is  $Z_*(x, y)$ , the the volumetric depth is

$$\Phi(\delta) = \frac{1}{A} \iint (\delta + Z_0 - Z_*(x, y)) H(\delta + Z_0 - Z_*(x, y)) dx dy \quad (1)$$

Where the integration is over the surface of the IWP,  $A$  is the area of the  
85 IWP,  $Z_0$  is the minimum elevation in the IWP, and  $H$  is the Heaviside  
function. This could be computed from the microtopography and stored as  
a lookup table. Or, we could employ a simpler parameterization. To that  
end, we consider parameterizing the microtopography with two parameters:  
(1) the elevation range spanned by the subgrid microtopography  $\delta_{\max}$ , and

90 (2) the specific excluded volume  $\delta_{\text{ex}}$ , which is the soil volume per unit bulk area. Then, we approximate the volumetric depth as

$$\Phi(\delta) = \begin{cases} (2\delta_{\text{max}} - 3\delta_{\text{ex}}) \left(\frac{\delta}{\delta_{\text{max}}}\right)^2 + (2\delta_{\text{ex}} - \delta_{\text{max}}) \left(\frac{\delta}{\delta_{\text{max}}}\right)^3 & \text{if } 0 \leq \delta \leq \delta_{\text{max}}, \\ \delta - \delta_{\text{ex}} & \text{if } \delta > \delta_{\text{max}}. \end{cases} \quad (2)$$

The volumetric depth calculated from the approximation (Equation 2) is compared (curve) with the direct calculation (Equation 1 (dots) ) for four ice-wedge polygon in Figure 2 and representative of other polygons. Also, shown is the volumetric depth in the absence of microtopography, which is linear with slope unity. Equation 1 is a very good approximation. Microtopographic effects on the flow law are not as straightforward to incorporate as the volumetric head  $\Phi(\delta)$ . In particular, we should make the distinction between depressions and obstructions (Panday and Huyakorn, 2004). Depressions are disconnected low points in the topography. The ponded depth must rise above the level of those depressions before any flow can happen. Obstructions exist above the depressions and interrupt and slow the flow, but do not block it completely. To model the effects of obstructions and depressions, we propose the following modification to the flow law

$$U = -\Theta(\delta) \frac{(\delta - \delta_{\text{d}})^{2/3}}{n_{\text{mann}}(\|\nabla Z\| + \epsilon)^{1/2}} \quad (3)$$

where  $\delta_{\text{d}}$  is the depression depth, and  $\Theta(\delta) \in [0, 1]$  is a fractional conductance which account for flow reduction by obstructions. polygons-finescale

To calculate  $\delta_{\text{d}}$  from the microtopography, we now propose an approach  
 95 based on site percolation. Specifically, we fill the lowest elevation surface cells until the cluster of inundated cells spans the IWP. This is the percolation threshold. The water height at the percolation threshold defines the

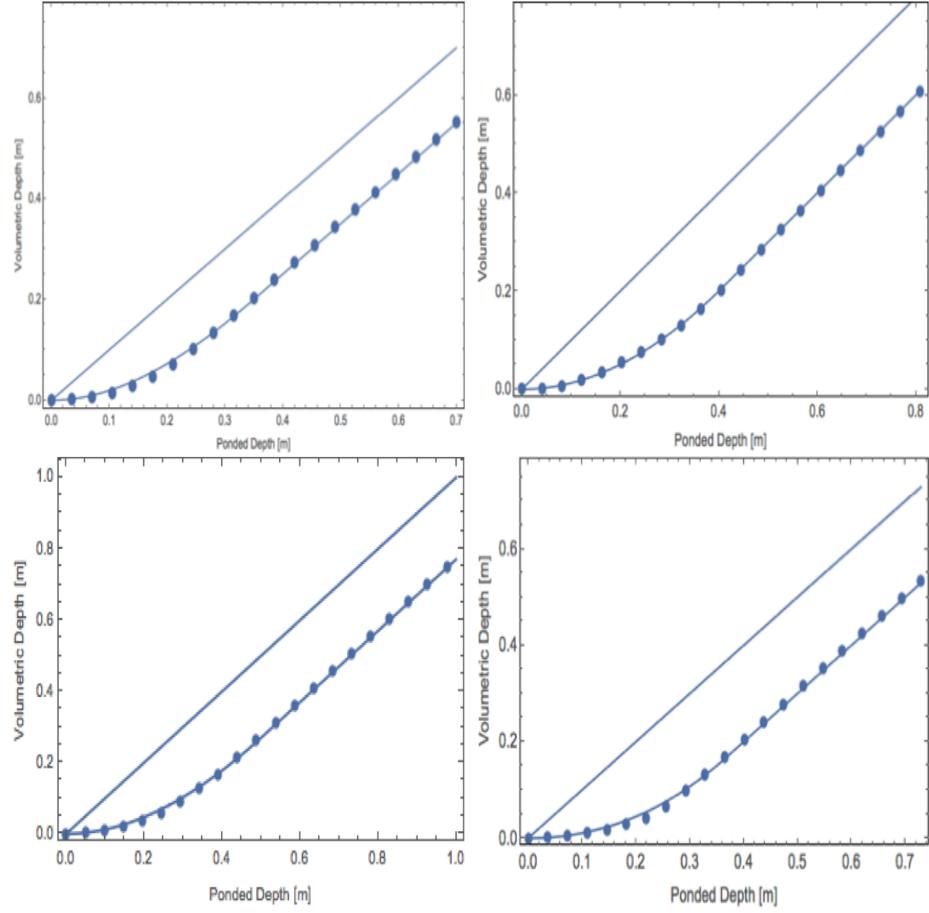


Figure 2: Volumetric depth versus ponded depth for four ice-wedge polygons. The ice-wedge polygons are displayed in Figure 4.



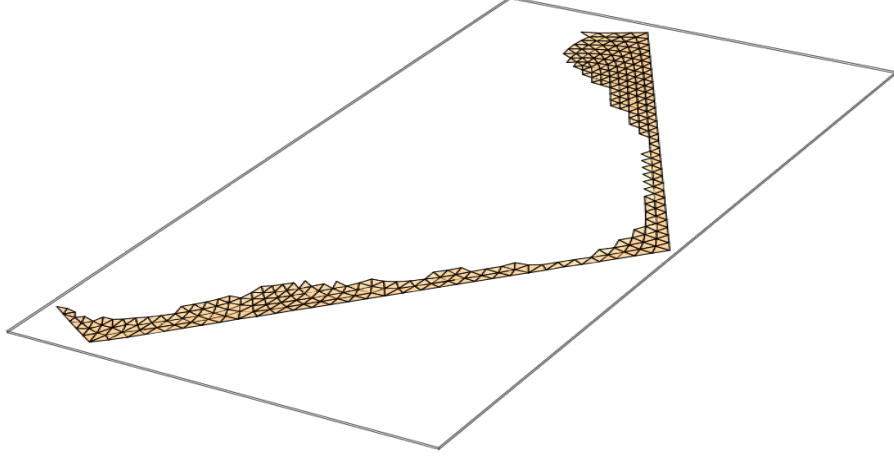


Figure 3: The spanning cluster at the percolation threshold for the IWP of Figure ?? . The water depth relative to the low point of the microtopography at the percolation threshold defines the depression depth.

$\delta_d$ . Figure 3 shows the spanning cluster at the percolation threshold for the IWP C40 shown in Figure 4. The depression depth calculated this way is 4.1  
 100 cm for this IWP. It is reasonable to assume that the fractional conductance is well approximated by the fractional cross section available to flow, which can be estimated as the ratio of volumetric depth to ponded depth.

$$\Theta(\delta_d) \approx \frac{(\Phi(\delta) - \Phi(\delta_d))}{\delta} H(\delta - \delta_d) \quad (4)$$

Where  $H$  is the Heaviside function. The numerator is the flowing cross sectional area. Note the velocity is multiplied by ponded depth to get a  
 105 flux, so the molar flux appearing in the conservation equations becomes

$$\eta_l \delta U = -\eta_l (\Phi(\delta) - \Phi(\delta_d)) H(\delta - \delta_d) \Theta(\delta) \frac{(\delta - \delta_d)^{2/3}}{n_{\text{mann}} (\|\nabla Z\| + \epsilon)^{1/2}} \nabla(Z + \delta) \quad (5)$$

In summary, we hypothesize that the microtopographic effects on surface flow can be captured with a simple approximation with three parameters that can be computed from the microtopography:

- Subgrid relief  $\delta_{\max} = Z_{*,\max} - Z_{*,\min}$ , where  $Z_{*,\max}$  and  $Z_{*,\min}$  are the maximum and minimum elevation in the microtopography.
- Specific excluded volume  $\delta_{\text{ex}}$ , the soil volume above the microtopographic low point normalized by IWP area.
- Depression depth  $\delta$ , the difference between the maximum and minimum elevation of the cells in the spanning cluster at the percolation threshold.

The subgrid relief and specific excluded volume come directly from the microtopography (univariate statistics). The depression depth requires a simple percolation algorithm to identify the spanning cluster at the percolation threshold. Values are given in Table 1.

Table 1: Parameters used in the subgrid model

	C06	C31	C40	C44	C45	A0	B01
$\delta_{\max}(m)$	0.404	0.262	0.483	0.364	0.350	0.361	0.411
$\delta_{\text{ex}}(m)$	0.2	0.105	0.23	0.2	0.15	0.185	0.26
$\delta_{\text{d}}(m)$	0.069	0.128	0.043	0.187	0.164	0.222	0.143

### 3. The Advanced Terrestrial Simulator (ATS)

Here we provide a very brief overview of the ATS for a reference, for more details about the software infrastructure we refer the reader to [17, 18].

125 A fully integrated surface/subsurface and snow distribution modeling ca-  
 pability implemented in ATS are available here [14, 19]. In addition, a  
 mixed-dimensional modeling strategy, mainly designed for the simulations  
 of low-relief permafrost-affected regions, can be found here [11]. The ATS  
 is a publically-available massively parallel computer code, an extended ver-  
 130 sion of Amanzi (flow and reactive transport simulator; see [20]), based on  
 process management tool called Arcos. In ATS, a proces kernel (PK) refers  
 to governing mathematical equations representing a particular (or coupled)  
 physical process(es). Further, Multiprocess Coordinators (MPCs) are avail-  
 able to facilitate coupling among PKs. This framework allows to dynam-  
 135 ically build a complex/coupled hierarchical model structure. The flexible  
 extensibility feature of the Arcos framework allowed to easily implement  
 our subgrid model and couple with the existing PKs.

## 4. Numerical Results and Discussions

### 4.1. Simulations

140 To assess the accuracy of the numerical results of our subgrid model, we  
 compare our results with fine-scale simulations and a coarsened model with-  
 out subgrid (hereinafter referred to as “no subgrid model”). For demonstra-  
 tion purpose, the comparison is made for surface-only flow simulations. In  
 our work, the seven ice-wedge polygon for fine-scale simulations are consid-  
 145 ered from Barrow Environmental Observatory (BEO) and illustrated in Fig-  
 ure 4. The ice-wedge polygons named A, B and C correspond to the NGEE  
 Arctic field sites A, B and C (see Figure 1), respectively. These polygons  
 consist of low-centered, high-centered, with well established troughs (rela-  
 tively uniform elevation across the trough) and obstructions in the troughs,

150 and hence represent a broader class of polygonal landscape. Three sets of numerical results of the subgrid model are presented:

**Study I:** Subgrid uncalibrated results;

**Study II:** Subgrid results with calibrated values of the depression depth listed in Table 1;

155 **Study III:** Subgrid simulations with calibrated values of the depression depth and a drag coefficient (Study II with drag factor).

Study II is motivated by fine-scale simulations, higher depression depth may delay breakthrough, and would lead to more accumulation of water in the depressions. That said, in Study II we adjust the value the depression  
160 depth computed by the percolation algorithm to provide a better fit to the fine-scale results. The process of adjusting model's parameters to replicate the benchmark (e.g., fine-scale computational or real experiments) results is known as calibration. Moreover, higher pressure in the subgrid model affects the overland conductivity and hence the discharge rate. To mimic  
165 the behavior of the fine-scale at the time of breakthrough and the recession period, the surface roughness is decreased by raising the manning coefficient in the governing equation. This analysis proposed Study III. Raising the manning coefficient is analogous to introducing a drag factor.

A pulse numerical test (injection followed by recession) is performed in  
170 all the numerical simulations presented. That is, we start with a fully dry surface, and inject water at a constant rate at the inlet boundary until breakthrough happens (prescribed flux boundary for a certain period of time), then stop the water supply and let water pass through the outlet (free drainage boundary). The arrows shown in Figure 4 indicate the inlet  
175 and outlet boundaries. To point out, the entire fine-scale IWP is considered

as one coarsened grid cell in the subgrid and no subgrid model – the elevation of faces depends on the elevation of the corners of the fine-scale IWP. It is important to mention that the higher (inlet) and lower (outlet) boundaries are chosen based on the average elevation of the faces in the coarsened grid.

180 For instance, the  $\text{inlet}_2$  in the coarsened grid of the polygon A01 (shown in Figure 4) is higher than the  $\text{outlet}_2$ , however, the fine-scale shows  $\text{inlet}_2$  is lower than  $\text{outlet}_2$ .

The rainfall events are not considered. The presence of depression depth parameter in the flow law of our subgrid model will not allow to replicate

185 the shape of the hydrograph because the fine-scale simulations will show immediate breakthrough. To capture such a behavior it would be more practical to determine the value of the depression depth dynamicly – change the depression depth as the ponded depth changes. This sort of research will be reported somewhere else.

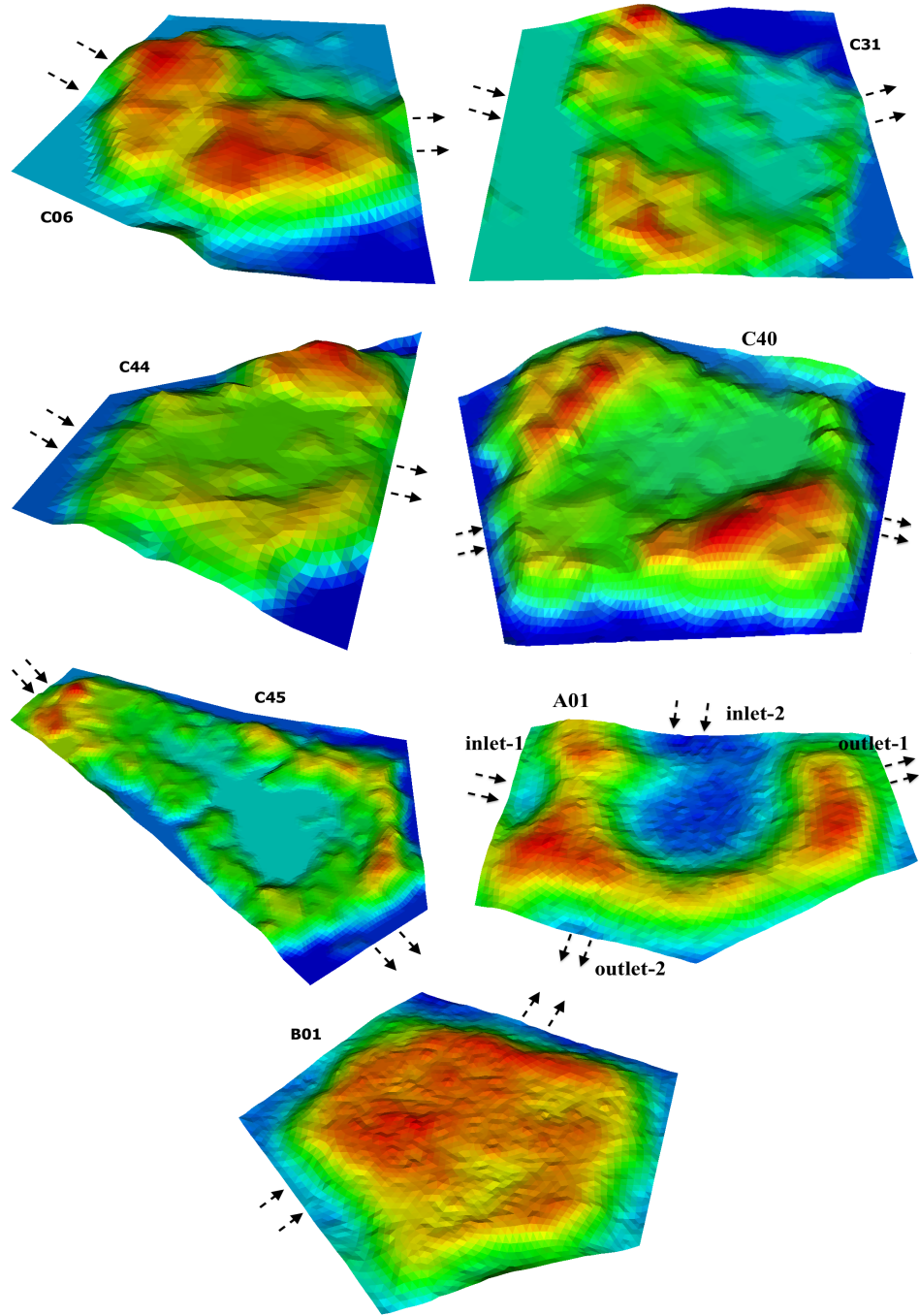


Figure 4: An Illustration of the microtopography of ice-wedge polygons from Barrow Environmental Observatory (BEO). Red and dark blue spots correspond to high- and low-elevated regions. The arrows indicate inlet and outlet boundaries.

190 *4.2. Results and Discussions*

Numerical results presented here correspond to the three studies mentioned above. We compare our results with fine-scale simulations of single IWPs, and we do not present any results on a cluster of fine-scale IWPs. We have carried out detailed simulations on all the polygons shown in Figure 4, however, we discuss the results of polygon C44 in more detail and these results serve as a representative of all the remaining polygons as far as the accuracy and shape of the hydrographs are concerned. Figure 5 compares the numerical results of the subgrid model with the fine-scale simulations, and no subgrid model of polygon C44. Clearly, Study I fails to match the fine-scale simulations, delayed breakthrough in the subgrid model is an indication of higher depression depth computed by the percolation algorithm; see Figure 5(a). Simulations with a calibrated depression depth, Study II, dramatically improve the shape of the hydrograph and the water content in the system as highlighted in see Figure 5(b). However, a mismatch appears at the time of breakthrough and the beginning of the recession period even with the calibrated depression depth. As alluded to earlier, this is due to the huge head gradient between the center and the seepage face, and physically makes sense. Figure 5(c) illustrates the results of Study III, and it is evident that our subgrid model reproduces the fine-scale behavior, and the numerical results are identical.

Figure 6 compares the numerical results of Study I and III with the fine-scale and no subgrid model. The percolation algorithm computed the depression depth very accurately for polygon C06, and calibration (Study II) is not required. Similar to the results of polygon C44, the high over-land conductivity in the subgrid model is reduced by increasing the surface roughness. It improves the results and replicate the recession period of the

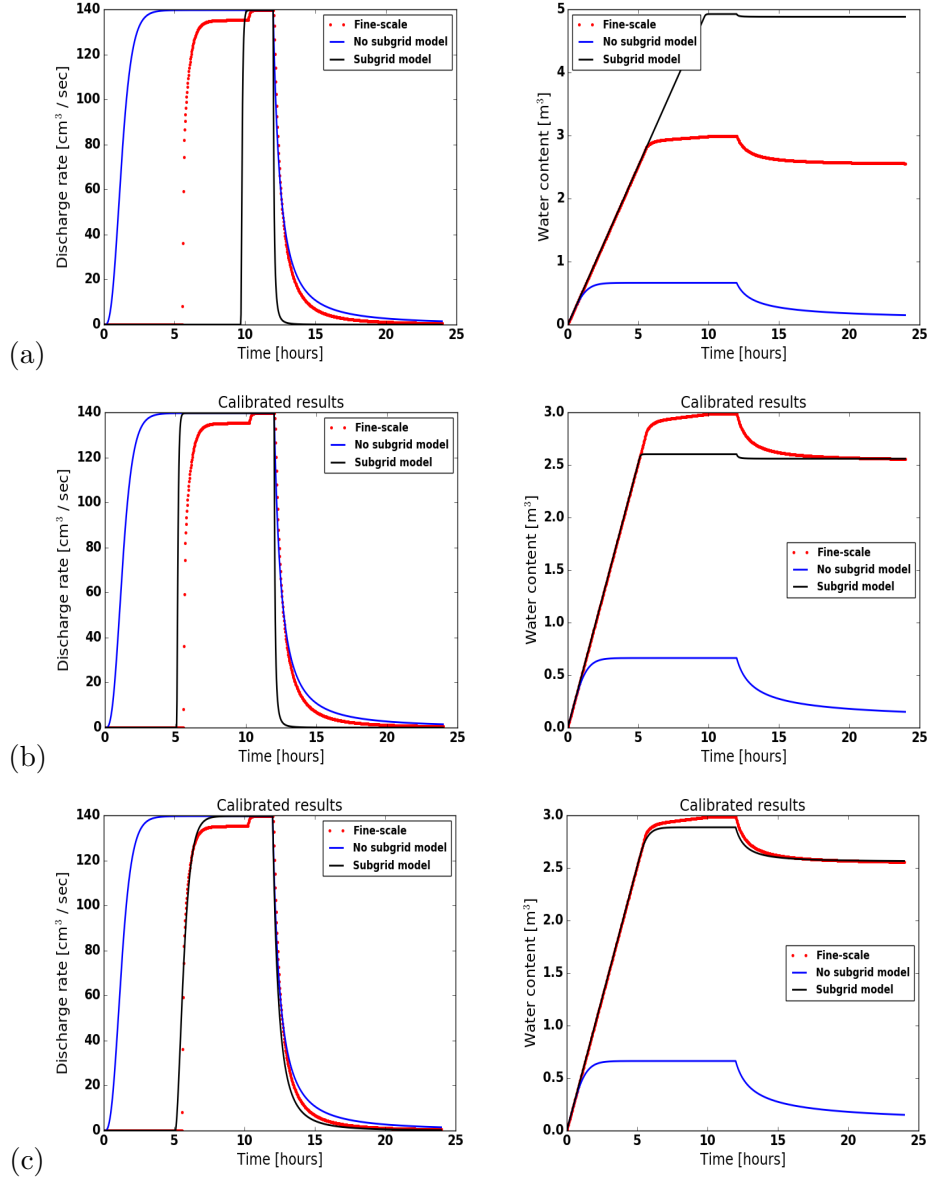


Figure 5: (Polygon C44) Comparison of the numerical results of the subgrid model with the fine-scale and without subgrid model results. Rows (top to bottom) correspond to Study I, II and III, respectively.



fine-scale results. It is important to see the amount of water (not available for drainage) in the system after the recession period. Figure 6 also displays the water retained the in subgrid model and the fine-scale model – the match is very close. For polygon C31, the results of the subgrid model are strongly affected by the depression depth in Study I, and lead to a mismatch. However, the results of Study II and III indicate that calibrated values of the depression depth and the surface roughness improved the simulated results dramatically and yield a close match as depicted in Figure 7. Numerical simulations correspond to polygons C31, C45, A01, and B01 are shown in Figures 7, 9, 10(a), and 11, respectively. Overall, the results of the subgrid model are very encouraging and consistently yield a better fit to the fine-scale results as compared to the no subgrid model.

#### 4.3. Additional Remarks

- Not surprisingly, the subgrid model favors high surface roughness that swings the results toward fine-scale simulations. A high agreement between the results of the subgrid model and fine-scale simulations due to reduced runoff is an indication of a needed drag coefficient in the flow law. A linear regression fit to the drag factor vs. the depression depth is depicted in Figure 12. The drag factor varies between zero and one, as the depression depth decreases the drag factor goes to unity – a representation of flow over a flat surface. The fit indicates the resistance to flow increases with increasing depression.
- For low-centered polygons such as C45 and A01, Study I (uncalibrated results) fails to match the hydrograph of the fine-scale simulations – no breakthrough happens for the uncalibrated depression depths. Fine-scale simulations show that low-elevated regions may remain com-

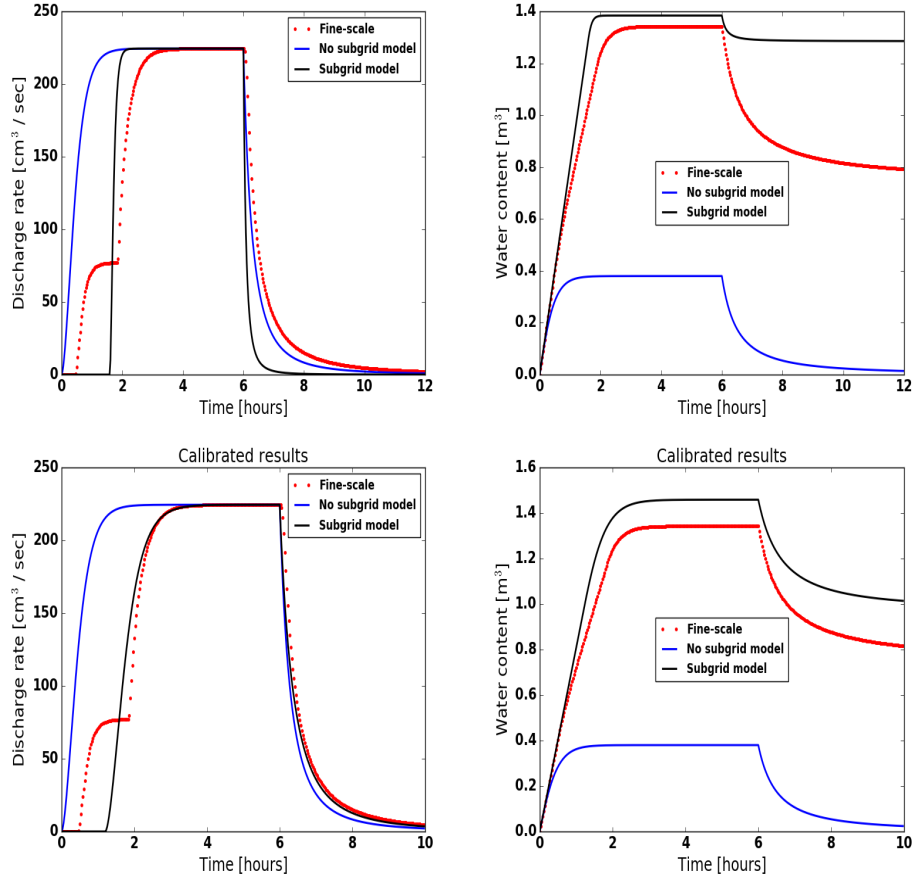


Figure 6: (Polygon C06) Comparison of the numerical results of the subgrid model with the fine-scale and without subgrid model results. Top and bottom row correspond to Study I and Study III, respectively.

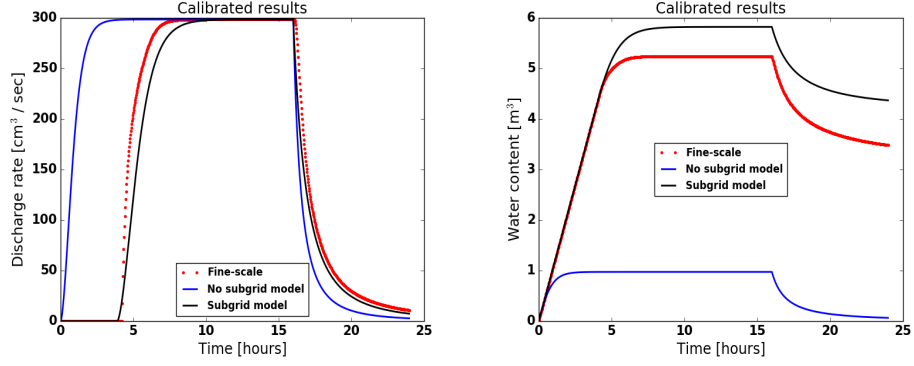


Figure 7: (Polygon C31) Comparison of the numerical results of the subgrid model with the fine-scale and no subgrid model. Results corresponded to Study III.

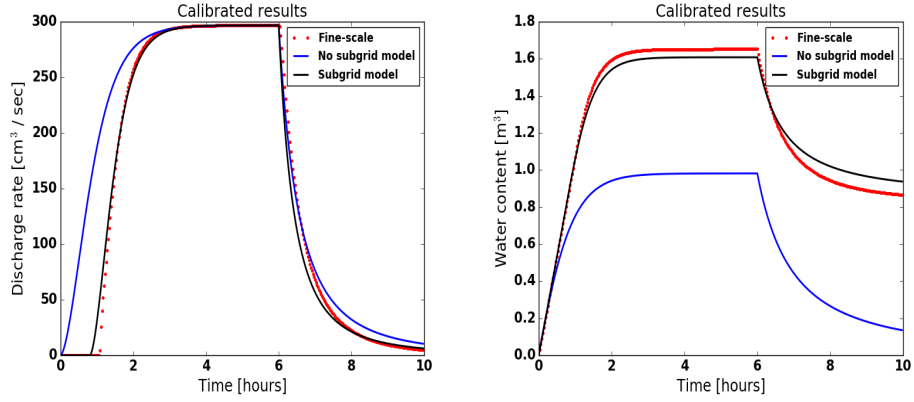


Figure 8: (Polygon C40) Comparison of the numerical results of the subgrid model with the fine-scale and without subgrid model results. Bottom row displays calibrated results.

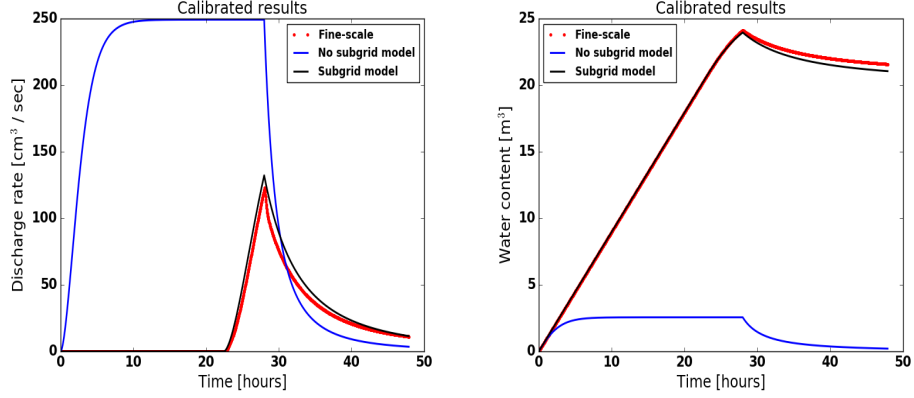


Figure 9: (Polygon C45) An illustration of the numerical results of the subgrid model, the fine-scale and no subgrid model. The simulations correspond to Study III.

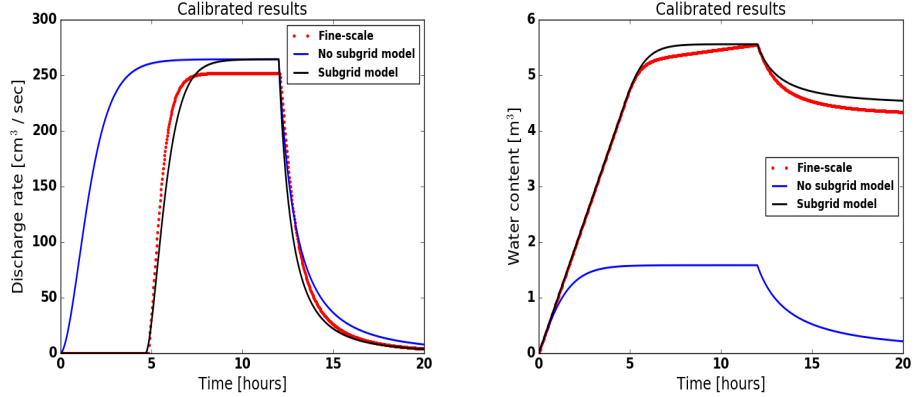


Figure 10: (Polygon A01) Comparison of the hydrographs and water content from the numerical simulation of the fine-scale, subgrid and no subgrid models.

pletely dry if they are not located in the main flow channel which trivial. However, as stated earlier, our percolation algorithm fills the lowest elevation cells until the cluster of inundated cells spans the IWP. Thereby, the direction of the injected fluid is important. For instance, considering polygon A01, the results are not comparable if the inlet

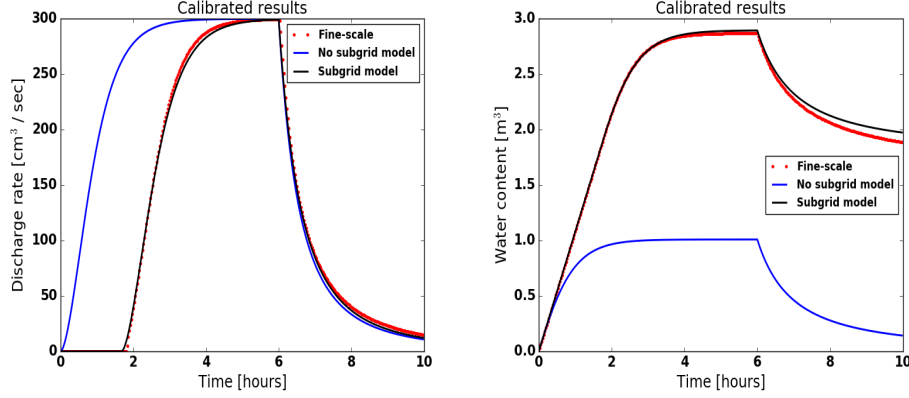


Figure 11: (Polygon B01) Comparison of the numerical results of the subgrid model with the fine-scale and without subgrid model results.

and outlet are at sides  $\text{inlet}_1$  and  $\text{outlet}_1$ , respectively. However, if the inlet and outlet are switched to  $\text{inlet}_2$  and  $\text{outlet}_2$  a desirable match is obtained; see Figure 13.

- Application of invaded percolation (flow in the direction of least resistance) algorithm could provide more accurate depression depths, and would probably overcome the issue of calibrating parameters and/or location of inlet and outlet boundaries.

- Most of our numerical experiments show that the subgrid model outperforms the no subgrid model even when the fine-scale flow behavior is not completely captured.

- When the inlet boundary has obstructions (for example, polygon C06 in Figure 4) and divides the incoming water into different flow channels, the water reaches the outlet boundary at different times and lead to a dual-peak (or may be multiple peaks) hydrograph. Due to only one grid cell in the subgrid model, the dual-peak behavior is not

possible to capture.

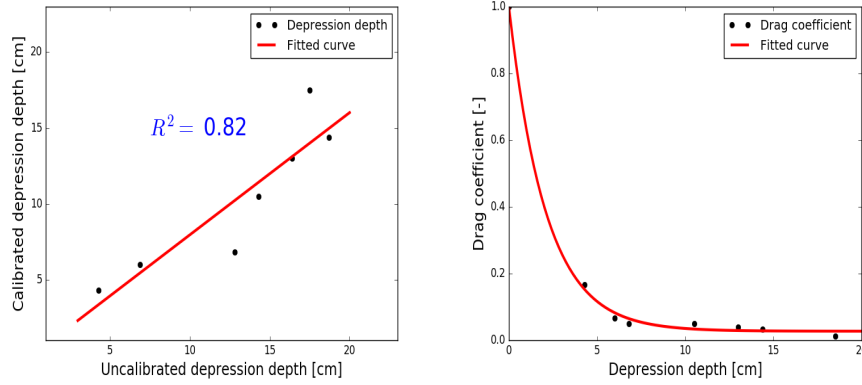


Figure 12: (Left) Linear fitted-curve to the depression depth data. (Right) Drag factor vs. calibrated depression depth. **LEFT FIG. NEEDS TO BE UPDATED**

## 5. Conclusions

265 The subgrid model presented in this paper is aimed at incorporating  
the microtopographic effects in the governing equations for the simu-  
lations at watershed-scale. The comparatively analysis of the subgrid  
results with the fine-scale IWP results reveal that our model has the  
potential to accurately represent fine-scale flow behavior at larger spa-  
270 tial scales. Numerical results of the subgrid model compare very well  
with the fine-scale simulations conducted on seven ice-wedge polygons.  
In addition, the model is applied to 468 polygons watershed and the  
results are physically consistent. More rigorous analysis is required to  
simultaneously capture both surface runoff and precipitation. More-  
275 over, invaded percolation could reduce the load of parameters calibra-  
tion.

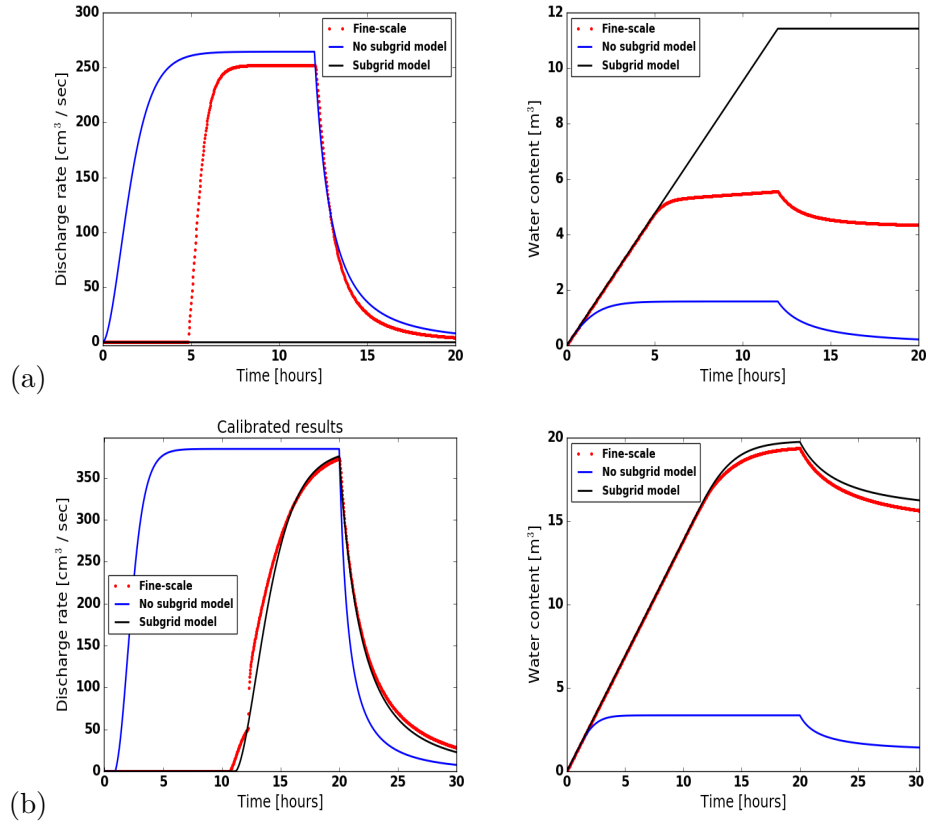


Figure 13: (Polygon A01) An illustration of the choice of the inlet and outlet boundaries on the numerical results. The orientation affects the match between the fine-scale and subgrid model. (a) inlet<sub>1</sub> and outlet<sub>1</sub> boundary; (b) inlet<sub>2</sub> and outlet<sub>2</sub> boundary.

## References

- [1] A. H. Lachenbruch, Mechanics of thermal contraction cracks and ice-wedge polygons in permafrost, Geological Society of America Special Papers 70 (1962) 1–66.
- [2] G. W. Greene, Contraction theory of ice-wedge polygons: A qualitative discussion, 1963.

- 285 [3] J. R. Mackay, Some observations on the growth and deformation of epigenetic, syngenetic and anti-syngenetic ice wedges, *Permafrost and Periglacial Processes* 1 (1990) 15–29.
- [4] J. Mackay, Thermally induced movements in ice-wedge polygons, western arctic coast, *Geomorphology: Critical Concepts in Geography* 5 (2004) 477.
- 290 [5] J. Kumar, N. Collier, G. Bisht, R. T. Mills, P. E. Thornton, C. M. Iversen, V. Romanovsky, Modeling the spatiotemporal variability in subsurface thermal regimes across a low-relief polygonal tundra landscape, *The Cryosphere* 10 (2016) 2241–2274.
- 295 [6] M. T. Jorgenson, Y. L. Shur, E. R. Pullman, Abrupt increase in permafrost degradation in arctic alaska, *Geophysical Research Letters* 33 (2006).
- [7] L. D. Hinzman, N. D. Bettez, W. R. Bolton, F. S. Chapin, M. B. Dyurgerov, C. L. Fastie, B. Griffith, R. D. Hollister, A. Hope, H. P. Huntington, et al., Evidence and implications of recent climate change in northern alaska and other arctic regions, *Climatic Change* 72 (2005) 251–298.
- 300 [8] J. C. Rowland, C. E. Jones, G. Altmann, R. Bryan, B. T. Crosby, L. D. Hinzman, D. L. Kane, D. M. Lawrence, A. Mancino, P. Marsh, J. P. McNamara, V. E. Romanvosky, H. Toniolo, B. J. Travis, E. Trochim, C. J. Wilson, G. L. Geernaert, Arctic landscapes in transition: Responses to thawing permafrost, *Eos, Transactions American Geophysical Union* 91 (2010) 229–230.
- 305



- [9] A. Liljedahl, L. Hinzman, J. Schulla, Ice-wedge polygon type controls low-gradient watershed-scale hydrology, in: Proceedings of the Tenth International Conference on Permafrost, volume 1, 2012, pp. 231–236.
- [10] J.-K. Huang, K. T. Lee, Influences of spatially heterogeneous roughness on flow hydrographs, *Advances in water resources* 32 (2009) 1580–1587.
- [11] A. Jan, E. T. Coon, P. S. L., R. Garimella, J. D. Moulton, An intermediate-scale model for thermal hydrology in low-relief permafrost-affected landscapes, Submitted to *Computational Geosciences* (2016).
- [12] S. Painter, J. Moulton, C. Wilson, Modeling challenges for predicting hydrologic response to degrading permafrost, *Hydrogeology Journal* (2013) 1–4.
- [13] B. L. Kurylyk, K. T. MacQuarrie, J. M. McKenzie, Climate change impacts on groundwater and soil temperatures in cold and temperate regions: Implications, mathematical theory, and emerging simulation tools, *Earth-Science Reviews* 138 (2014) 313–334.
- [14] S. L. Painter, E. T. Coon, A. L. Atchley, M. Berndt, R. Garimella, J. D. Moulton, D. Svyatskiy, C. J. Wilson, Integrated surface/subsurface permafrost thermal hydrology: Model formulation and proof-of-concept simulations, *Water Resources Research* 52 (2016) 6062–6077.

- [15] W. N. Stammers, H. Ayers, The effect of slope and microtopography on depression storage and surface detention, publisher not identified, 1956.
- [16] S. Panday, P. S. Huyakorn, A fully coupled physically-based spatially-distributed model for evaluating surface/subsurface flow, *Advances in water Resources* 27 (2004) 361–382.
- [17] E. T. Coon, J. D. Moulton, S. L. Painter, Managing complexity in simulations of land surface and near-surface processes, *Water Resources Research* 78 (2016) 134–149.
- [18] E. T. Coon, *ATS: The Advanced Terrestrial Simulator*, 2016. <http://github.com/amanzi/ats>.
- [19] A. L. Atchley, S. L. Painter, D. R. Harp, E. T. Coon, C. J. Wilson, A. K. Liljedahl, V. E. Romanovsky, Using field observations to inform thermal hydrology models of permafrost dynamics with ats (v0.83), *Geoscientific Model Development* 8 (2015) 2701–2722.
- [20] J. D. Moulton, M. Berndt, R. Garimella, L. Prichett-Sheats, G. Hammond, M. Day, J. Meza, High-level design of amanzi, the multi-process high performance computing simulator, office of environmental management, united states department of energy, washington dc (2012).